Regenerative Engineering and Translational Medicine (2021) 7:301–311
https://doi.org/10.1007/s40883-019-00138-x

Gelatin-Based Microribbon Hydrogels Guided Mesenchymal Stem Cells to Undergo Endochondral Ossification In Vivo with Bone-Mimicking Mechanical Strength

Bogdan Conrad[1] · Camila Hayashi[2] · Fan Yang[3,4]

Received: 8 July 2019 / Revised: 14 October 2019 / Accepted: 19 October 2019 / Published online: 10 December 2019

Abstract

Most stem cell–based bone tissue engineering strategies to date yield bone through direct bone formation, which mimics intramembranous ossification. However, bone injuries often affect long bones which are formed through endochondral ossification, involving an initial cartilage template formation followed by remodeling to form bones. There remains a critical need to develop scaffolds that enhance stem cell–based bone formation through endochondral ossification with bone-mimicking mechanical strength. Here we evaluated the potential of gelatin-based microribbons (μRBs) as macroporous scaffolds for enhancing human mesenchymal stem cell (MSC)–based bone formation through endochondral ossification. This material platform was compared with conventional gelatin hydrogels (HGs) as controls. MSCs were encapsulated in μRB or HG scaffolds, primed in chondrogenic medium in vitro for 2 weeks, and then implanted in a mouse subcutaneous model with no additional factors. μRB scaffolds supported fast cartilage deposition by MSCs, which was completely remodeled and replaced by mineralized bone. Impressively, the compressive moduli of MSC-seeded μRB scaffolds increased from 10 to 3224 kPa by week 11, a range that mimics native bone. In comparison, while HG supported endochondral ossification, the speed was much slower, with less matrix deposition and only a modest increase in compressive modulus to 269 kPa. These results validate gelatin μRBs as a promising scaffold for repairing long bone defects by guiding robust endochondral ossification.

Lay Summary

Natural bone development and healing occurs through two distinct pathways: intramembranous ossification and endochondral ossification. Most bone injuries affect long bones, which are formed through endochondral ossification, involving an initial cartilage template formation followed by remodeling to form bones. However, scaffolds that can guide stem cell–based bone formation through endochondral ossification with bone-mimicking mechanical strength remain lacking. Here we report that macroporous gelatin-based microribbons (μRBs) accelerate endochondral ossification by human mesenchymal stem cells (MSCs) in vivo using a mouse subcutaneous model. Impressively, the mechanical properties of MSC-seeded μRB scaffolds

Electronic supplementary material The online version of this article (https://doi.org/10.1007/s40883-019-00138-x) contains supplementary material, which is available to authorized users.

✉ Fan Yang
fanyang@stanford.edu

Bogdan Conrad
bconrad4@stanford.edu

Camila Hayashi
camilah@stanford.edu

[1] Program of Stem Cell Biology and Regenerative Medicine, Stanford University School of Medicine, 300 Pasteur Dr., Edward Building Room 114, Stanford, CA 94305, USA

[2] Department of Chemical Engineering, Stanford University School of Engineering, Shriram Center, Room 129, Stanford, CA 94305, USA

[3] Department of Orthopaedic Surgery, Stanford University School of Medicine, 300 Pasteur Dr., Edward Building Room 114, Stanford, CA 94305, USA

[4] Department of Bioengineering, Stanford University, 300 Pasteur Dr., Edward Building Room 114, Stanford, CA 94305, USA

increased over 300-fold over 11 weeks to bone-mimicking range, whereas conventional gelatin hydrogel controls reached less than 10% of the bone modulus. These results validate gelatin μRBs as a promising novel scaffold for repairing long bone defects by guiding robust endochondral ossification.

Keywords Macroporous · Scaffolds · Endochondral ossification · Bone · Stem cells · Gelatin · Microribbon

Introduction

Bone loss affects millions of patients annually and can be caused by trauma, cancer resections, or degenerative diseases such as osteoporosis and osteonecrosis [1–4]. Bone is the second most commonly transplanted tissue after blood [5]. Given the donor scarcity and potential immunogenicity associated with bone grafts, there remains a significant need for alternative treatment options for repairing critical size bone defects that cannot heal on their own [1]. Depending on the anatomical locations, bones in the human body form and heal through two distinct processes: intramembranous ossification or endochondral ossification [6–8]. Flat bones in skull, mandible, maxilla, and clavicles form through intramembranous ossification, which is characterized by direct bone formation [9]. Long bones that make up most of the skeleton, on the other hand, are formed through endochondral ossification. While intramembranous ossification results in direct bone formation, endochondral ossification involves formation of an intermediate avascular cartilage template, which is subsequently remodeled and replaced by vasculature ingrowth and bone tissue [10–12].

To promote bone regeneration, various biomaterials have been employed including ceramics, poly(ester)-based scaffolds, and hydrogels [13]. Despite the extensive efforts and progress in utilizing biomaterials to enhance bone regeneration, most strategies developed to date resulted in direct bone formation [14–18], which only mimics flat bones formed through intramembranous ossification. The majority of bone fractures, however, occur in long bones, which are formed through endochondral ossification with a cartilage template. To induce endochondral ossification, recent studies primed mesenchymal stem cells (MSCs) in chondrogenic medium containing TGF-β3 in vitro for 2 to 5 weeks before in vivo implantation using a rodent subcutaneous model. This protocol was shown to induce cartilage template formation in vitro, which was subsequently remodeled and replaced by mineralized bone in vivo [19, 20]. However, several limitations remain. First, the previous method required additional factors such as cartilage-derived matrix particles or IL-1β [19, 20]. Second, the speed of bone formation remains very slow, requiring up to 14 weeks to achieve only partial mineralization [20, 21]. Third, these studies have been unable to achieve bone-mimicking mechanical strength, characterized by high stiffness in the range of MPa [22, 23] due to slow and limited mineralization.

To facilitate clinical translation, the ideal scaffold for MSC-based bone regeneration should support direct and homogenous cell encapsulation, contain macroporosity to accelerate new matrix deposition, and facilitate rapid increase in the mechanical properties of resulting bone. While conventional hydrogels support easy cell encapsulation, they generally contain porosity orders of magnitude smaller than cells, leading to physical restriction and slow tissue formation [24–26]. Although porosity can be introduced into hydrogels using porogens, this further reduces the already weak mechanical properties of hydrogels [27]. Conventional methods for fabricating macroporous scaffolds, such as PLGA sponges, do not support direct cell encapsulation. To overcome the limitations associated with conventional biomaterials for bone regeneration, our lab has recently reported a method to fabricate gelatin into microribbon (μRB)–shaped hydrogel building blocks featuring widths (40–100 μm) larger than the size of individual cells, which support homogeneous cell encapsulation, as shown by confocal microscopy, and can subsequently intercrosslink to form 3D macroporous cell-laden scaffolds [25, 28]. Unlike conventional hydrogels, the resulting μRB scaffolds exhibit great shock-absorbing capacity and maintain structural integrity upon cyclic compression [25, 26, 28]. We further demonstrated that the macroporosity of μRB scaffolds made with 7.5% (w/v) μRBs substantially accelerated stem cell–based cartilage regeneration in vitro [26] and enhanced stem cell survival and endogenous bone formation in vivo [25]. However, the potential of gelatin μRB scaffolds to support MSC-based endochondral ossification has yet to be explored. Here we seek to compare gelatin μRB scaffolds to gelatin hydrogel (HG) scaffolds for their potential to guide MSC-based bone formation via endochondral ossification. We hypothesized that the macroporosity within μRB scaffolds would accelerate and enhance new bone formation and result in a faster increase in mechanical strength of engineered bone tissue. To induce the formation of an intermediate cartilaginous template, human MSCs were encapsulated in both μRB and HG scaffolds and cultured in chondrogenic medium supplemented with TGF-β3 for 2 weeks. The scaffolds were then implanted subcutaneously in nude mice for up to 9 additional weeks in vivo without any additional growth factors. The resulting tissues were characterized at multiple time points using mechanical testing, histology, and immunostaining.

Materials and Methods

Materials

Dimethyl sulfoxide (DMSO), L-lysine hydrochloride, gelatin type-A (Bloom number range: 90 to 300 g), methacrylic anhydride, and glutaraldehyde were purchased from Sigma-Aldrich (St. Louis, MO). All materials were used as received.

Scaffolds Fabrication and Characterization

Methacrylated gelatin was synthesized as previously described for forming conventional hydrogels [26]. Gelatin μRBs (40–100 μm wide, 2–3 mm long, and about 4 μm thick) were fabricated using wet-spinning as previously reported [26]. Both μRB and HG scaffolds (2 mm in height and 4.5 mm in diameter) were formed using the same concentration of gelatin (7.5% w/v) and photocrosslinked, induced by a photoinitiator (LAP, 0.05% w/v) and UV light (365 nm, 2 mW/cm^2, 4 min) [28]. Scaffold morphology was characterized using scanning electron microscopy with a Hitachi S-3400N variable pressure scanning electron microscope [26]. The sample stage was cooled gradually from room temperature to operating temperature (− 25 °C); simultaneously, the chamber pressure was reduced from 1 atm to 50 Pa, following a pressure-temperature curve at which water stays in the liquid phase, to ensure samples remained hydrated and did not dry or freeze. Images were taken using an electron beam of 15 kV at a working distance of ~ 7 mm.

Cell Encapsulation in 3D

Human MSCs (Lonza, Basel, Switzerland) were expanded in standard MSC growth medium [26] until passage 6 before use for encapsulation. MSCs were encapsulated in either gelatin μRBs or gelatin HGs at 15 million cells/ml. The same gelatin concentration (7.5% w/v) was used for both μRB and HG groups. The cell/polymer mixture was loaded between two glass slides (with a 2 mm spacer) and crosslinked by UV light (365 nm, 2 mW/cm^2, 4 min). After 24 h of incubation in MSC growth medium, cylindrical samples (4.5 mm in diameter) were punched out using a biopsy punch and transferred to 24-well plates. Cell viability 24 h after encapsulation was evaluated using a LIVE/DEAD Viability/Cytotoxicity Kit (Invitrogen, Carlsbad, CA). Images were acquired using a Zeiss fluorescence microscope (Axio Observer 3.1, Zeiss, Oberkochen, Germany) and the ZEN 2 (blue edition) software (Zeiss).

In Vitro Priming and In Vivo Implantation

To induce endochondral ossification, all cell-laden scaffolds were first primed in vitro for 2 weeks in chondrogenic medium containing high-glucose DMEM, 10 ng/ml of TGF-β3, 100 nM of Dexamethasone, 50 μg/ml of ascorbic-2-phosphate, 40 μg/ml of proline, 5 μg/ml of ITS premix, 100 μg/ml of sodium pyruvate, 100 units/ml of penicillin, and 100 μg/ml of streptomycin [26], followed by subcutaneous implantation in vivo using an immunocompromised mouse model (NCRNU, female, 9 weeks, Taconic). All animal studies were performed in accordance with the National Institutes of Health guide for the care and use of Laboratory animals (NIH Publications No. 8023, revised 1978); all protocols were approved by the Stanford institutional animal care and use committee. Samples were harvested at multiple time points (2, 5, and 11 weeks from the initial encapsulation) for analyses. Outcomes were analyzed using mechanical testing (n = 5/group), histology, and immunostaining (n = 3/group).

Histology and Immunostaining

In vivo samples showed excellent host-tissue integration and hence scaffolds were harvested with peripheral host tissue, as especially the μRB samples were impossible to separate from the fibrous capsule. At the time of each harvest time point, all samples were fixed in 4% paraformaldehyde (4 °C, 2 h), embedded in optimal cutting temperature (OCT) compound (VWR International, Radnor, PA), and frozen using liquid nitrogen vapor. A Microtome Cryostat (Triangle Biomedical Sciences, Durham, NC) was used to cut 8 μm-thick sections from the OCT-embedded samples. Safranin-O staining (Sigma-Aldrich) was used to visualize sulfated glycosaminoglycan (sGAG) deposition. Collagen deposition and tissue morphology was examined with Masson's trichrome staining (Thermo Scientific, Waltham, MA). Alkaline phosphatase (ALP) staining was visualized using Fast Blue RR Salt (FBS25, Sigma-Aldrich) and Naphthol AS-MX phosphate (855, Sigma-Aldrich). Mineralization was stained using Alizarin Red S (ARS) (A5533, Sigma-Aldrich). For immunostaining, sections were blocked with 2% goat serum and 3% bovine serum albumin in 1X PBS for 1 h and incubated overnight at 4 °C in the presence of diluted primary antibodies. The following antibodies were used: rabbit polyclonal antibodies against collagen I (ab34710, 1:100, Abcam, Cambridge, MA), collagen II (ab34712, 1:80, Abcam), collagen X (ab58632, 1:100, Abcam), and osteopontin (ab8448, 1:100, Abcam); and rat polyclonal antibodies against osteocalcin (ab13418, 1:80, Abcam), F4/80 (MCA497GA, 1:50, Bio-Rad, Hercules, CA), or vimentin (ab92547, 1:200, Abcam). Depending on the primary antibodies of choice, the following secondary antibodies were used: Alexa Fluor 488 goat anti-rabbit (1:100, Invitrogen) and Alexa Fluor 488 goat anti-rat (1:100, Invitrogen). Samples were also incubated without primary antibodies and only secondary antibodies as negative controls. Nuclei were counter stained using Hoechst 33342 (Thermo Scientific). Images were taken with a Zeiss

fluorescence microscope (Axio Observer 3.1) and the ZEN 2 (blue edition) software (Zeiss).

Mechanical Testing

Unconfined compression tests were conducted using an Instron 5944 system (Instron Corporation, Norwood, MA) fitted with a 10 N load cell (Interface Inc., Scottsdale, AZ). Sample constructs were tested on the following timepoints: weeks 0, 2, 5, and 11 (n = 3–5 per time point). The setup consisted of custom-made aluminum compression platens lined with polytetrafluoroethylene to minimize friction. All tests were conducted in PBS at room temperature. Before each test, a preload of approximately 10 mN was applied. The upper plate was then lowered at a rate of 1% strain/s to a maximum strain of 30%. Load and displacement data were recorded at 100 Hz. The compressive modulus was calculated from a linear curve fit of the stress versus strain curve within the range of 20–30%.

Statistical Analysis

All data were expressed as mean ± standard error. Statistical significance was determined via analysis of variance using Student's t test with equal variance. p values (two-tailed) < 0.05 were considered statistically significant, and p values < 0.005 were considered statistically highly significant.

Results

µRB Scaffolds Accelerated Matrix Deposition by MSCs and Exhibited Faster Degradation In Vivo

To induce endochondral ossification, MSC-seeded µRB and HG scaffolds were first cultured in vitro in chondrogenic medium containing TGF-β, then implanted in a mouse subcutaneous model without any growth factors for up to 9 additional weeks (Fig. 1A). Acellular µRB and HG groups were included as negative controls. LIVE/DEAD staining showed high cell viability and homogeneous cell distribution in both groups 24 h after encapsulation (Fig. 1B). Cells encapsulated in the µRB scaffolds showed extensive spreading on the surface of the ribbons but remained round and entrapped in HG (Fig. 1B). The observed cell distribution and morphology corroborated whole sample confocal microscopy results published previously [25]. SEM showed that µRB scaffolds exhibited a highly interconnected macroporous network, whereas HG contained much smaller and restrictive pores (Fig. 1C).

Visual examination of sample gross morphology over time reveals that MSC-seeded µRB scaffolds showed a more rapid increase in opacity than HG over time, suggesting that µRBs supported faster new matrix deposition by MSCs compared with HG (Fig. 1D). MSC-seeded µRB scaffolds became white and shiny by week 5, resembling the appearance of articular cartilage. (Fig. 1D). In contrast, acellular µRB scaffolds

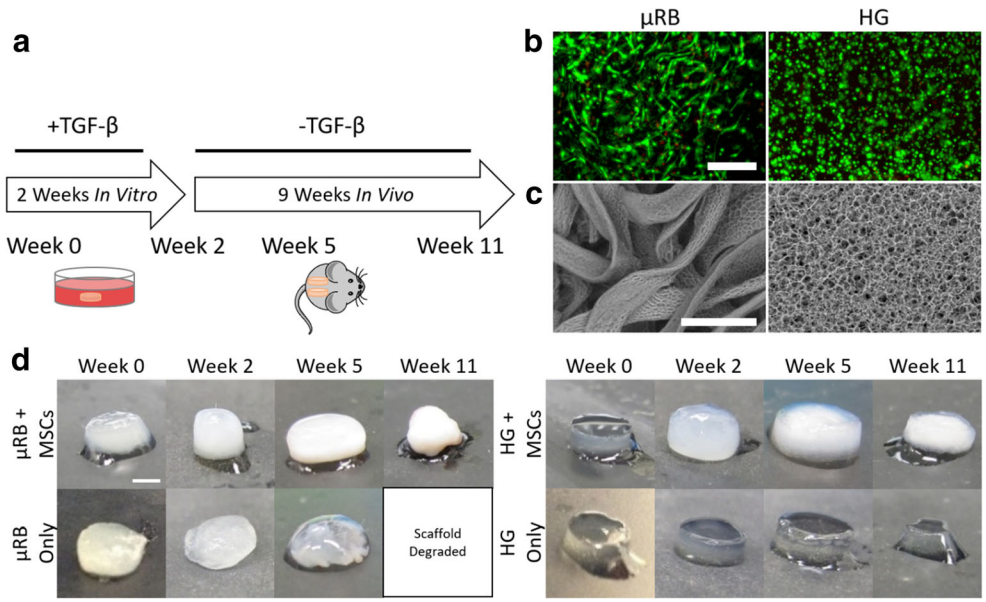

Fig. 1 Experimental design and characterization of gelatin-based µRB scaffolds vs. conventional HGs as a 3D stem cell niche. (A) Schematic of in vivo experimental design. Human MSCs were encapsulated in gelatin µRB or HG scaffolds and first cultured in chondrogenic medium containing TGF-β3 for 2 weeks in vitro. The samples were then implanted in a mouse subcutaneous model without additional growth factors. Samples were harvested at weeks 5 and 11 for analysis. (B) Cell viability and morphology in µRB and HG scaffolds 24 h after encapsulation as shown by LIVE/DEAD staining. Green: live cells; red: dead cells; scale bar 200 µm. (C) SEM to compare the macroporosity in the µRB and HG scaffolds. Scale bar 100 µm. (D) Gross morphology of µRB and HG scaffolds with or without MSCs over time. Increase in sample opacity indicates matrix deposition. Scale bar 2 mm

quickly degraded over time, becoming transparent by week 5. By week 11 they could not be found, suggesting full degradation (Fig. 1D). While the MSC-seeded HGs also showed increasing opacity over time, the degree of opacity was much less compared with the MSC-seeded μRB scaffolds, suggesting HGs induced less and slower matrix deposition (Fig. 1D). In addition, the newly deposited matrix was not as homogeneous in HGs, as the opacity was higher in the center of HGs, leaving a transparent edge. Acellular HG samples remained transparent throughout the duration of the experiment, showing partial degradation by week 11 (Fig. 1D).

MSC Seeded μRB Scaffolds, but Not HGs, Enabled Fast Increase in Compressive Moduli of Engineered Tissues over Time

Given that weight bearing is an important function of bone tissue, we next characterized the changes in compressive modulus of MSC-seeded μRB scaffolds or HG scaffolds over time using unconfined compression testing. At week 0, all samples exhibited low compressive moduli, with ~ 6–10 kPa for μRB scaffolds, and higher for HG scaffolds (~ 23–40 kPa) (Fig. 2). After 2 weeks of in vitro culture in chondrogenic medium containing TGF-β, the compressive modulus of MSC-containing μRB scaffolds increased 21-fold, reaching 210 kPa, whereas MSC-seeded HGs only increased slightly to 47 kPa (Fig. 2). Acellular μRB scaffolds degraded substantially, accompanied by a decrease in compressive modulus to ~ 2 kPa (Fig. 2). No significant changes were observed in compressive modulus of acellular HGs (Fig. 2).

Following subcutaneous implantation, the compressive modulus of MSC-seeded μRBs or HGs showed a minor change between weeks 2 and 5, followed by a huge increase between weeks 5 and 11. By week 11, the compressive modulus of MSC-seeded μRBs reached an impressive 3224 kPa (Fig. 2), which is comparable to the compressive modulus of native bone tissue [22, 23]. In contrast, acellular μRB samples had fully degraded by this point. MSC-seeded HGs showed a smaller increase to 270 kPa by week 11, less than 10% of the compressive modulus of the MSC-seeded μRBs (Fig. 2). Compared with week 0, MSC-seeded μRB and HG scaffolds exhibited a total of 325-fold and 12-fold increase in compressive modulus, respectively (Fig. 2). Given the same amount of gelatin was used for making μRB or HG scaffolds, macroporous μRB scaffolds were much more efficient in enabling rapid increase of mechanical strength of new bone tissues deposited by MSCs in 3D.

Macroporous μRB Scaffolds Accelerated Cartilage Deposition and Subsequent Remodeling In Vivo

To assess whether μRB and HG scaffolds can support temporary cartilage formation and subsequent remodeling in vivo, samples were harvested at weeks 5 and 11 and stained for cartilage matrix. Safranin-O staining was used to visualize the amount and distribution of sGAGs, a key component of cartilage matrix. Low magnification images were shown to illustrate the matrix distribution throughout the scaffolds, and high magnification images were shown for assessing matrix distribution on the cellular level. By week 5, μRB + MSC scaffolds were completely filled with sGAGs distributed in a highly interconnected manner, but sGAGs were almost completely absent by week 11 (Fig. 3A). In contrast, the HG + MSC group only showed a small amount of sGAG deposition by week 5, limited to the center of the sample, which continued to increase by week 11 (Fig. 3A). Acellular scaffolds were also stained and showed no sGAGs at any time point (Fig. S1A), confirming all sGAGs were deposited by encapsulated MSCs, not host cells.

To view total collagen deposition, Masson's Trichrome staining was performed on all samples. A fibrous capsule can be found around the edge of scaffolds in all groups over time (Fig. 3B, Fig. S1B). Unlike the trend of sGAGs, collagen deposition showed a continuous increase in both μRB + MSC and HG + MSC groups, with the newly deposited matrix filling up the pores in the scaffolds (Fig. 3B). Since the scaffolds are gelatin-based, which stains positive for Masson's Trichrome, we also included acellular samples to show the

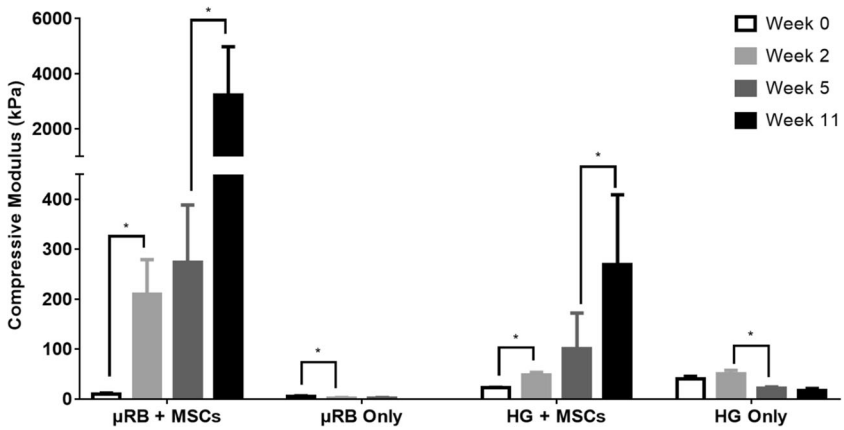

Fig. 2 Characterization of compressive moduli of gelatin μRB scaffolds or gelatin HGs, with or without MSCs over 11 weeks using unconfined compressive testing. The compressive moduli of the acellular μRB group were not performed at week 11 due to complete sample degradation. *$p < 0.05$

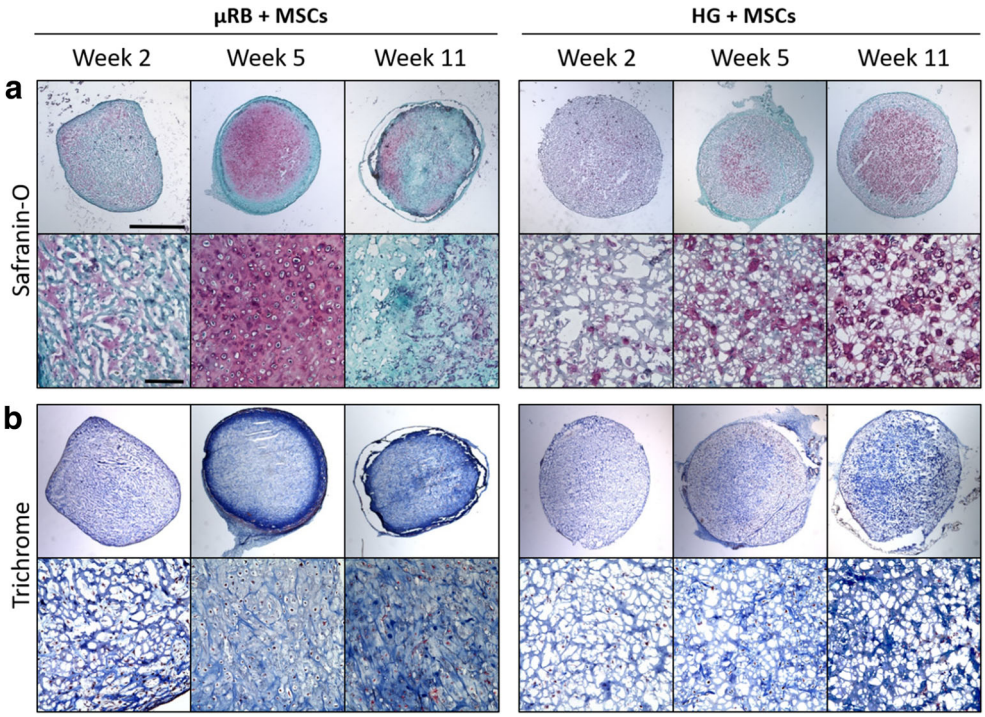

Fig. 3 Gelatin μRB scaffolds accelerated the speed and amount of new tissue matrix deposition compared with HGs over time. (A) Safranin-O staining for sGAGs, a major component of articular cartilage; (B) Masson's Trichrome staining for total collagen. Low magnification (upper row) and high magnification (lower row) images are provided for both stains. Scale bars in low magnification images: 1 mm; scale bars in high magnification images: 200 μm

background due to the scaffolds. Only scaffold structures similar to SEM results were observed (Fig. S1B), confirming the majority of collagen filling the spaces throughout the macropores were contributed by MSC-deposited new matrix.

To further characterize the cartilage phenotype, immunostaining was performed for type II collagen (a marker for desirable articular cartilage), type X collagen (hypertrophic cartilage marker) and type I collagen (fibrocartilage or bone marker) (Fig. 4, S2). For MSC-seeded μRBs, type II collagen increased at week 2, peaked at week 5, but largely disappeared by week 11 (Fig. 4A). A similar trend was observed for type X collagen (Fig. 4B). Collagen I started to be positive at week 5, and continued to increase by week 11 (Fig. 4C). A similar trend of phenotype change was observed in the HG + MSC group, but the amount of matrix was much less than in the μRB + MSC group and limited to only the pericellular regions (Fig. 4). Acellular samples showed no background staining in any sample (Fig. S2), confirming all matrix was contributed by transplanted MSCs, not by host cells.

μRB Scaffold Accelerated Endochondral Ossification by MSCs In Vivo

The disappearance of cartilage markers (sGAG and type II/X collagen) after week 5, combined with the increase in type I collagen by week 11, suggested a phenotype transition of

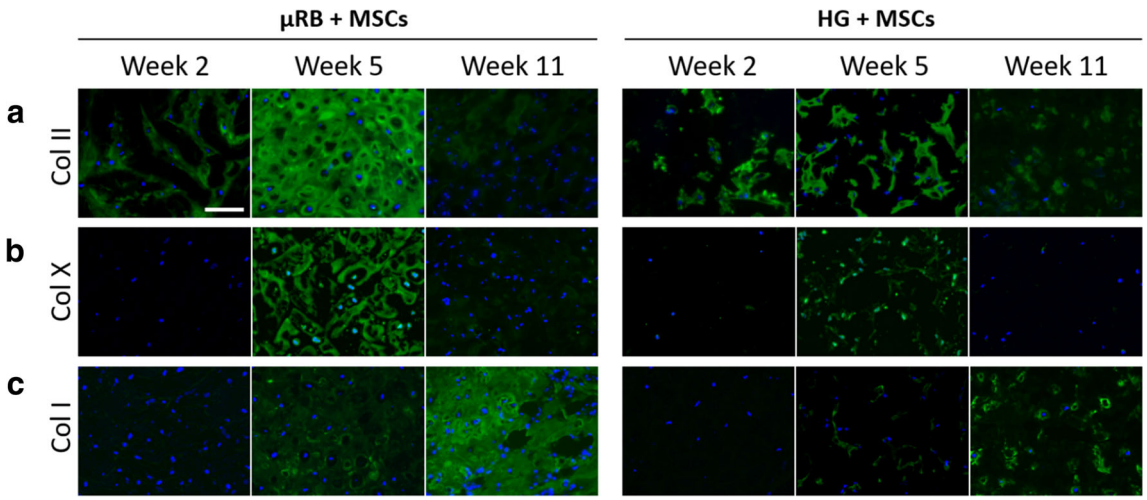

Fig. 4 Immunostainings of different types of collagen deposited by MSCs showed gelatin μRB scaffolds accelerated endochondral ossification compared with HGs. (A) Type II collagen, (B) type X collagen, (C) type I collagen. Green: specific type of collagen; blue: nuclei. Scale bar 100 μm

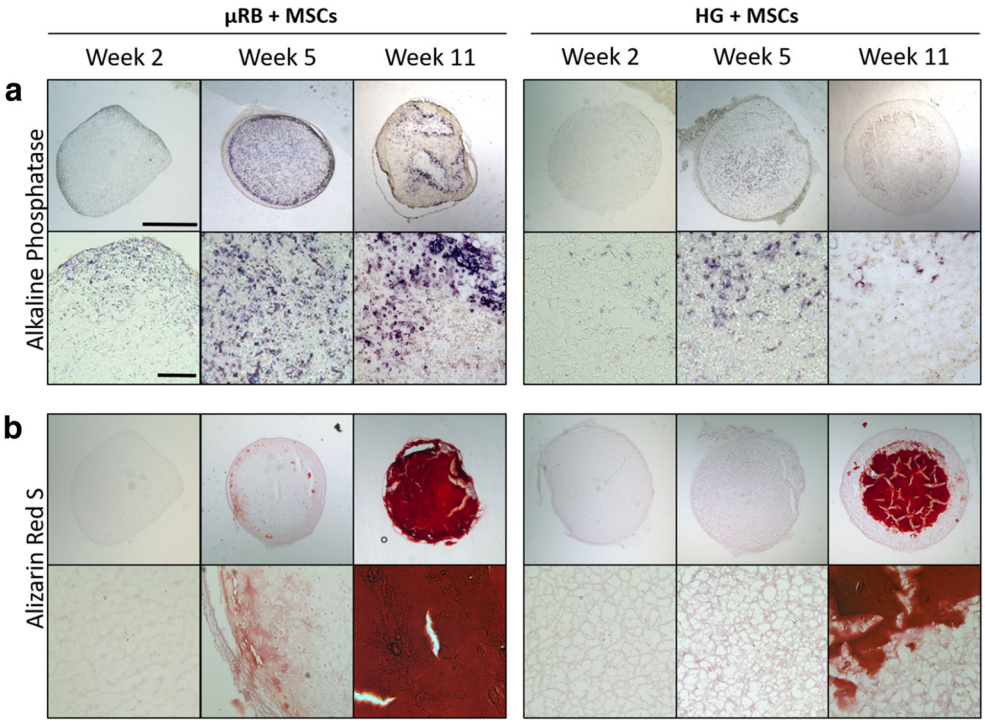

Fig. 5 Staining of bone markers showed gelatin μRB scaffolds accelerated mineralized bone formation over time compared with gelatin HG. (A) ALP, an early bone marker; (B) ARS staining for mineralization. Upper row: low magnification, scale bar 1 mm; lower row: high magnification, scale bar 200 μm

MSC-deposited tissues from cartilage to bone between weeks 5 and 11 (Figs. 3 and 4). To further confirm the bone phenotype, all samples were stained for ALP, an early bone marker, as well as mineralization using ARS staining. For the μRB + MSC group, ALP increased substantially at week 5 and decreased by week 11 (Fig. 5A). ARS staining shows that mineralized bone started to emerge in the periphery of MSC-seeded μRBs at week 5 and filled the entire scaffold with intense mineralization by week 11 (Fig. 5B). The HG + MSC sample showed delayed bone formation, with no mineralization observed at week 5, and intense mineralization was observed by week 11 but limited to only the center of the sample (Fig. 5A, B). Acellular control samples were negative for ALP and ARS for all samples at all timepoints (Fig. S3).

To further characterize the speed of bone formation, we performed immunostaining for osteopontin and osteocalcin, which are intermediate and late bone markers respectively (Fig. 6, S4). Consistent with the histology results, immunostaining shows that μRBs supported a much faster transition to bone phenotype than HGs, as both markers were expressed much earlier in the μRB samples (Fig. 6). Acellular samples showed no signals at any timepoints (Fig. S4).

Characterization of Host Cell Infiltration In Vivo

In vivo samples were harvested with the surrounding host tissues intact as the macroporosity of μRB scaffolds induced rapid host tissue ingrowth, leading to excellent host tissue integration and difficulty in separating the implants from the surrounding host tissue. Histological staining from samples harvested at weeks 5 and 11 demonstrated a very distinctive in vivo response between μRB and HG scaffolds (Fig. 7). Masson's Trichrome staining showed a fibrous capsule formation around both cellular and acellular μRB and HG scaffolds (Fig. 3B, S1B). To further characterize the phenotype of these cells, samples were stained with F4/80, a marker for macrophages. The border of the μRB and HG scaffolds were marked with a white dotted line (Fig. 7A). While a small number of invading cells in the acellular μRB sample were F4/80 positive, the majority of cells in all groups were not macrophages

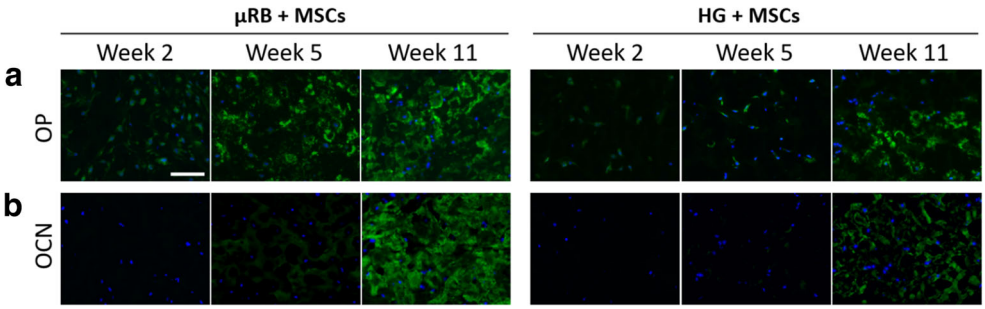

Fig. 6 Immunostainings of osteopontin and osteocalcin showed μRB scaffolds accelerated MSC osteogenesis and bone maturation compared with HGs. (A) Osteopontin; (B) osteocalcin. Scale bar 100 μm

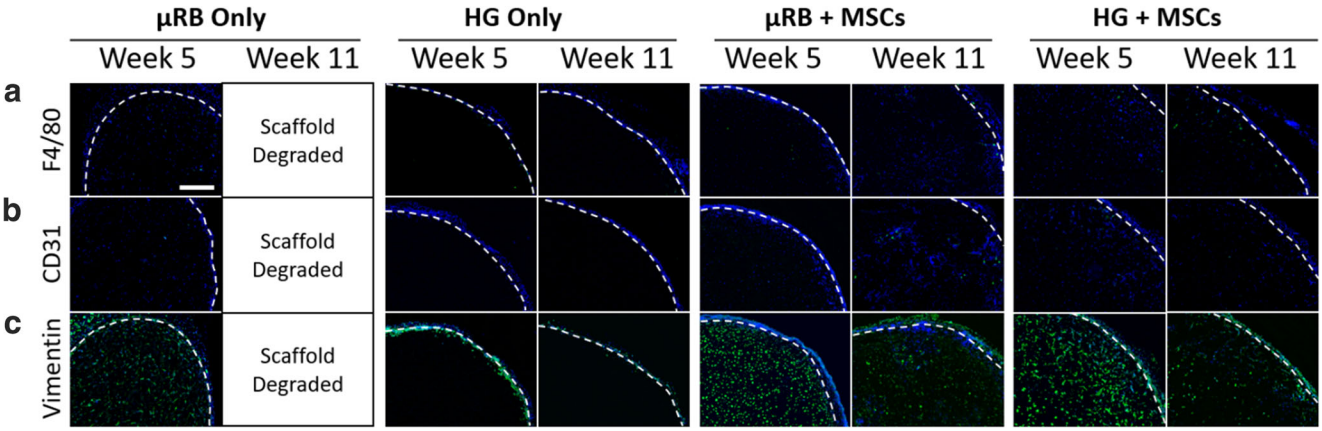

Fig. 7 Characterization of host cell infiltration into gelatin μRB scaffolds and gelatin HGs in a mouse subcutaneous model. Immunostaining was performed for markers for macrophages (F4/80), endothelial cells (CD31), and fibroblastic/mesenchymal cells (vimentin). White dotted line indicates the boundary of scaffolds. (A) F4/80; (B) CD31; (C) Vimentin. Scale bar 100 μm

(Fig. 7A). Staining with the endothelial marker CD31 for blood vessel invasion was also largely negative except for the μRB + MSC group at week 11 (Fig. 7B). Staining with vimentin revealed that the large majority of cells migrating into the μRB scaffold or forming the fibrous capsule around the HG were fibroblastic/mesenchymal cells (Fig. 7C). Endogenous cells were unable to invade into the acellular HG samples, suggesting that the vimentin positive cells in the HG + MSC group are encapsulated MSCs rather than host cells (Fig. 7C). In both cellular samples (μRB and HG), the vimentin signal decreased within the scaffold between weeks 5 and 11. Together, these results indicate that macroporous μRB scaffolds, but not HGs, enabled rapid host cell infiltration into the scaffolds, which is desirable for promoting host tissue integration (Fig. 7).

Discussion

Here we report that macroporous gelatin μRB scaffolds support MSC-based endochondral ossification in vivo with short in vitro priming in chondrogenic medium and no additional growth factors in vivo. Only gelatin μRB scaffolds, but not conventional HGs, enabled a fast increase in compressive modulus, first to the range of articular cartilage [29] and then to bone-mimicking stiffness (~ 3 MPa) [30] (Fig. 2). In addition, the macroporous μRB scaffold improved the homogenous distribution of de novo deposited cartilage and bone matrix throughout the scaffold (Figs. 3, 4, 5, and 6). These results support our hypothesis that the macroporosity within the μRB scaffold would accelerate and enhance matrix formation by MSCs in 3D, enabling faster restoration of mechanical strength of engineered tissues. Together, this study validates the efficacy of gelatin-based μRB scaffolds in supporting MSC-based bone regeneration through endochondral ossification and its substantial advantages over conventional gelatin HGs.

Most bone defects impact long bones, which are formed through endochondral ossification. Ideal scaffolds for stem cell–based bone repair for long bone defects should support the cartilage to bone phenotype transition while supporting rapid restoration of bone-mimicking mechanical strength. While some studies demonstrated endochondral ossification, none have reported achievement of mechanical strength in the range of native bone [19, 31–33]. Hydrogels in particular have shown limited success, with engineered bone tissue demonstrating compressive moduli an order of magnitude lower than that of native bone [34, 35]. This is consistent with our findings, where MSC-seeded HGs achieved less than 10% of the compressive moduli of native bone after 11 weeks (Fig. 2). In contrast, the macroporous gelatin μRB scaffold achieved cartilage-mimicking strength (210 kPa) after 2 weeks of culture in vitro and increased to a bone-mimicking compressive modulus by week 11 (3224.3 kPa) (Fig. 2). This increase is remarkable considering that the μRB scaffold alone is characterized by a compressive modulus of only ~ 10 kPa. Given that the HG and μRB scaffolds were made from the same concentration of gelatin, this stark contrast in the quality of new bone highlights the importance of scaffold design. The inherent interconnected macroporosity in the gelatin μRB scaffold reduces the physical restrictions experienced by cells in HGs, supporting fast cell spreading and interconnectivity of newly deposited matrix as shown by histology (Figs. 3, 4, 5, and 6). μRBs not only accelerated the speed of matrix deposition but also promoted a denser and more interconnected matrix network; in contrast, the matrix was limited to isolated pericellular deposition in HGs. Due to the extensive infiltration of host cells into the μRB scaffolds, it was not feasible to separate μRB implants from surrounding host tissues for accurate biochemical quantification, so we chose histology rather than biochemical assays to more accurately characterize the

tissue formation. Consistent with the findings from the present study, our previous in vitro study comparing the μRB and HG scaffolds for chondrogenesis also showed that macroporous gelatin μRB scaffolds substantially accelerate cartilage regeneration by MSCs with great interconnectivity compared with gelatin HGs [26]. Importantly, the fold of increase in mechanical property was much higher than the fold of change in total matrix content [26], confirming the improved interconnectivity is critical for improved mechanical function of engineering tissues. Since histology data shows distinct differences in both the amount and distribution of newly deposited tissues (Figs. 3, 4, 5, and 6) between μRB vs. HG groups, it is a much more reliable and accurate way to analyze in vivo tissue formation in this study.

To assess the biocompatibility and host integration of μRBs in vivo, we characterized host cell infiltration into the scaffolds using immunostainings for markers of macrophages (F4/80), endothelial cells (CD31), and fibroblastic/mesenchymal cells (vimentin). We observed minimal signals for macrophages and endothelial cells across all groups at both time points (weeks 5 and 11) (Fig. 7). The absence of detectable macrophages may be due to the relatively late time points, which passed the duration of the initial acute inflammatory phase. The absence of vasculature at week 5 is not surprising given that cartilage formation peaked at week 5. Cartilage is an avascular tissue and is known to secrete anti-angiogenic factors [36, 37]. With the remodeling of the cartilaginous template and formation of bone by week 11, we observed an increasing number of CD31-positive cells in the μRB scaffold. This is consistent with previous reports that angiogenesis plays a role in bone formation and fracture healing [10]. Endothelial cells were only observed in the μRB + MSC group, suggesting that both macroporosity and the presence of MSCs are necessary to promote vascular ingrowth. MSCs have been known to secrete a broad spectrum of paracrine signals that promote angiogenesis [38–40]. The fact that the HG + MSC group did not show any endothelial cell infiltration suggests the lack of macroporosity in conventional gelatin HGs inhibits host cell infiltration. This is further supported by the results of immunostaining of vimentin, which is an intermediate filament protein that is expressed in mesenchymal cells such as fibroblasts [41]. While acellular μRBs showed extensive staining of vimentin-positive cells throughout the scaffolds at week 5, acellular HGs completely inhibited cell infiltration throughout 11 weeks. For successful cartilage tissue regeneration, host tissue integration is essential, which requires rapid host cell infiltration. Our results validate that gelatin μRB scaffolds, but not HGs, are a much better choice for host tissue integration enhancement.

When characterizing biomaterials for in vivo applications, one important factor to consider is degradation. Ideally, the scaffold should degrade over time as the new tissue forms. Acellular μRB scaffolds degraded much faster than HGs and could not be retrieved by week 11 (Figs. 1D and 7). In contrast, acellular gelatin HGs showed minimal degradation. Given both scaffolds were made from the same concentration and composition (gelatin), the observed drastic difference in degradation is likely a result of differences in the macroporosity and speed of host cell infiltration (Fig. 7). As noted above, μRB scaffolds enabled rapid host cell infiltration and tissue integration while HGs inhibited host cell infiltration. Furthermore, the μRB scaffolds started to lose integrity as the intercrosslinks among μRB building blocks degraded, exposing increased surface area to infiltrated or transplanted cells which further accelerated the degradation of individual μRBs.

Another finding from this study is that transient priming of MSCs in chondrogenic medium containing TGF-β3 (2 weeks in vitro) was sufficient to induce MSCs to undergo endochondral ossification in vivo without the use of any additional growth factors. The simplicity of the protocol deems it highly desirable for clinical translation as it avoids cost for additional growth factors that suffer from short half-lives in vivo and can induce undesirable excessive bone formation [42]. Similar to our findings, previous studies have shown 2 to 5 weeks of in vitro priming in chondrogenic conditions was sufficient to induce endochondral ossification in a mouse subcutaneous model without additional growth factors [19, 21].

Conclusion

In summary, here we demonstrated that macroporous gelatin μRB scaffolds accelerated and enhanced endochondral ossification of human MSCs in vivo without the need for additional growth factors in vivo. The resulting tissue-engineered bone exhibited a rapid increase in mineralization and reached bone-mimicking mechanical strength. Unlike conventional HGs, μRBs exhibited a toothpaste-like texture when hydrated in PBS for injection, which makes it easier to apply for filling irregular-shaped defects in vivo than liquid hydrogel precursors. Given that macroporous μRB scaffolds induced rapid and extensive host cell infiltration, they also show great advantage in promoting host tissue integration, which is highly desirable for tissue engineering scaffolds. In the present study we have used a mouse subcutaneous model to demonstrate proof of principle given it is a more cost-effective and higher throughput choice and allowed testing of samples with larger sizes. Now that we have proven the advantages of gelatin μRBs over conventional HGs, future studies can further validate the potential of μRBs for supporting endochondral ossification using long bone defect models [31, 32, 43, 44].

Acknowledgments We thank Dr. Lydia-Marie Joubert from the Cell Sciences Imaging Facility at Stanford for use of, and assistance with, the Hitachi electron microscope. Finally, we thank Anthony Behn from

the Department of Orthopedic Surgery at Stanford for his assistance with mechanical testing.

Funding Information The authors would like to thank NIH R01DE024772-01 (F. Y.), National Science Foundation CAREER award program (CBET-1351289) (F. Y.), California Institute for Regenerative Medicine Tools and Technologies award (Grant #TR3-05569) (F. Y.), Stanford Chem-H Institute New Materials for Applications in Biology and Medicine Seed Grant (F. Y.), Stanford Child Health Research Institute (F. Y.), California Institute for Regenerative Medicine predoctoral fellowship (B. C.), and NIH NRSA predoctoral fellowship (5F31DE025788-03) (B. C.) for support.

Compliance with Ethical Standards

Ethical Approval All applicable international, national, and/or institutional guidelines for the care and use of animals were followed. All procedures performed in studies involving animals were in accordance with the ethical standards of the institution or practice at which the studies were conducted.

References

1. Schemitsch EH. Size matters: defining critical in bone defect size! J Orthop Trauma. 2017;31:S20–S2. https://doi.org/10.1097/bot.0000000000000978.
2. Health UDo, Services H. Bone health and osteoporosis: a report of the Surgeon General. Rockville, MD: US Department of Health and Human Services, Office of the Surgeon General. 2004;87.
3. Pollak AN, Watkins-Castillo SI. Fracture Trends. United States Bone and Joint Initiative: the burden of musculoskeletal diseases in the United States (BMUS). Third Edition ed. Rosemont, IL2014.
4. Aarvold A, Smith JO, Tayton ER, Jones AMH, Dawson JI, Lanham S, et al. A tissue engineering strategy for the treatment of avascular necrosis of the femoral head. Surgeon. 2013;11(6):319–25. https://doi.org/10.1016/j.surge.2013.02.008.
5. Van Heest A, Swiontkowski M. Bone-graft substitutes. Lancet. 1999;353(Supplement 1):S28–S9. https://doi.org/10.1016/S0140-6736(99)90228-3.
6. Cunningham C, Scheuer L, Black S. Chapter 3 - Bone Development. In: Developmental Juvenile Osteology. 2nd ed. San Diego: Academic Press; 2016. p. 19–35.
7. G SF. Developmental Biology. 6th ed. Sunderland: Sinauer Associates; 2000.
8. Marsell R, Einhorn TA. The biology of fracture healing. Injury. 2011;42(6):551–5. https://doi.org/10.1016/j.injury.2011.03.031.
9. Karaplis AC. Chapter 3 - Embryonic development of bone and regulation of intramembranous and endochondral bone formation A2 - Bilezikian, John P. In: Raisz LG, Martin TJ, editors. Principles of Bone Biology. 3rd ed. San Diego: Academic Press; 2008. p. 53–84.
10. Hadjiargyrou M, O'Keefe RJ. The convergence of fracture repair and stem cells: interplay of genes, aging, environmental factors and disease. J Bone Mine Res. 2014;29(11):2307–22. https://doi.org/10.1002/jbmr.2373.
11. Kronenberg HM. Developmental regulation of the growth plate. Nature. 2003;423:332–6. https://doi.org/10.1038/nature01657.
12. Maes C, Kronenberg HM. Chapter 60 - Bone development and remodeling A2 - Jameson, J. Larry. In: Groot LJ, Kretser DMD, Giudice LC, Grossman AB, Melmed S, Potts JT, et al., editors. Endocrinology: adult and pediatric. 7th ed. Philadelphia: W.B. Saunders; 2016. p. 1038–62.e8.
13. Ghassemi T, Shahroodi A, Ebrahimzadeh MH, Mousavian A, Movaffagh J, Moradi A. Current concepts in scaffolding for bone tissue engineering. Arch Bone Joint Surg. 2018;6(2):90–9.
14. Nii M, Lai JH, Keeney M, Han L-H, Behn A, Imanbayev G, et al. The effects of interactive mechanical and biochemical niche signaling on osteogenic differentiation of adipose-derived stem cells using combinatorial hydrogels. Acta Biomater. 2013;9(3):5475–83. https://doi.org/10.1016/j.actbio.2012.11.002.
15. Castillo Diaz LA, Elsawy M, Saiani A, Gough JE, Miller AF. Osteogenic differentiation of human mesenchymal stem cells promotes mineralization within a biodegradable peptide hydrogel. J Tissue Eng. 2016;7:2041731416649789. https://doi.org/10.1177/2041731416649789.
16. Ojansivu M, Johansson L, Vanhatupa S, Tamminen I, Hannula M, Hyttinen J, et al. Knitted 3D scaffolds of polybutylene succinate support human mesenchymal stem cell growth and osteogenesis. Stem Cells Int. 2018;2018:11. https://doi.org/10.1155/2018/5928935.
17. Pandit V, Zuidema JM, Venuto KN, Macione J, Dai G, Gilbert RJ, et al. Evaluation of multifunctional polysaccharide hydrogels with varying stiffness for bone tissue engineering. Tissue Eng Part A. 2013;19(21-22):2452–63. https://doi.org/10.1089/ten.TEA.2012.0644.
18. Wang X-F, Lu P-J, Song Y, Sun Y-C, Wang Y-G, Wang Y. Nano hydroxyapatite particles promote osteogenesis in a three-dimensional bio-printing construct consisting of alginate/gelatin/hASCs. RSC Adv. 2016;6(8):6832–42. https://doi.org/10.1039/C5RA21527G.
19. Visser J, Gawlitta D, Benders KEM, Toma SMH, Pouran B, van Weeren PR, et al. Endochondral bone formation in gelatin methacrylamide hydrogel with embedded cartilage-derived matrix particles. Biomaterials. 2015;37(Supplement C):174–82. https://doi.org/10.1016/j.biomaterials.2014.10.020.
20. Scotti C, Piccinini E, Takizawa H, Todorov A, Bourgine P, Papadimitropoulos A, et al. Engineering of a functional bone organ through endochondral ossification. Proc Natl Acad Sci U S A. 2013;110(10):3997–4002. https://doi.org/10.1073/pnas.1220108110.
21. Mikael PE, Xin X, Urso M, Jiang X, Wang L, Barnes B et al.. A potential translational approach for bone tissue engineering through endochondral ossification. 2014 36th Annual International Conference of the IEEE Engineering in Medicine and Biology Society; 2014 26-30 Aug. 2014.
22. Ravaglioli A, Krajewski A. Bioceramics: Materials Properties Applications: Springer Science & Business Media; 2012.
23. Hench LL. Bioceramics: from concept to clinic. J Am Ceram Soc. 1991;74(7):1487–510.
24. Hollister SJ. Porous scaffold design for tissue engineering. Nat Mater. 2005;4(7):518–24. https://doi.org/10.1038/nmat1421.
25. Han LH, Conrad B, Chung MT, Deveza L, Jiang X, Wang A, et al. Winner of the Young Investigator Award of the Society for Biomaterials at the 10th World Biomaterials Congress, May 17-22, 2016, Montreal QC, Canada: Microribbon-based hydrogels accelerate stem cell-based bone regeneration in a mouse critical-size cranial defect model. J Biomed Mater Res A. 2016;104(6):1321–31. https://doi.org/10.1002/jbm.a.35715.
26. Conrad B, Han LH, Yang F. Gelatin-based microribbon hydrogels accelerate cartilage formation by mesenchymal stem cells in 3D. Tissue Eng Part A. 2018;0(ja):null. https://doi.org/10.1089/ten.TEA.2018.0011.
27. Dadsetan M, Hefferan TE, Szatkowski JP, Mishra PK, Macura SI, Lu L, et al. Effect of hydrogel porosity on marrow stromal cell phenotypic expression. Biomaterials. 2008;29(14):2193–202. https://doi.org/10.1016/j.biomaterials.2008.01.006.
28. Han L-H, Yu S, Wang T, Behn AW, Yang F. Tissue Engineering: Microribbon-like elastomers for fabricating macroporous and

highly flexible scaffolds that support cell proliferation in 3D (Adv. Funct. Mater. 3/2013). Adv Funct Mater. 2013;23(3):266. https://doi.org/10.1002/adfm.201370014.
29. Athanasiou KA, Rosenwasser MP, Buckwalter JA, Malinin TI, Mow VC. Interspecies comparisons of in situ intrinsic mechanical properties of distal femoral cartilage. J Orthop Res. 1991;9(3):330–40. https://doi.org/10.1002/jor.1100090304.
30. Oftadeh R, Perez-Viloria M, Villa-Camacho JC, Vaziri A, Nazarian A. Biomechanics and mechanobiology of trabecular bone: a review. J Biomech Eng. 2015;137(1):010802.
31. Rentsch C, Rentsch B, Breier A, Spekl K, Jung R, Manthey S, et al. Long-bone critical-size defects treated with tissue-engineered polycaprolactone-co-lactide scaffolds: a pilot study on rats. J Biomed Mater Res A. 2010;95A(3):964–72. https://doi.org/10.1002/jbm.a.32878.
32. Viateau V, Guillemin G, Bousson V, Oudina K, Hannouche D, Sedel L, et al. Long-bone critical-size defects treated with tissue-engineered grafts: a study on sheep. J Orthop Res. 2007;25(6):741–9. https://doi.org/10.1002/jor.20352.
33. Sasaki J-I, Matsumoto T, Egusa H, Matsusaki M, Nishiguchi A, Nakano T, et al. In vitro reproduction of endochondral ossification using a 3D mesenchymal stem cell construct. Integr Biol. 2012;4(10):1207–14. https://doi.org/10.1039/C2IB20027A.
34. Chung C, Beecham M, Mauck RL, Burdick JA. The influence of degradation characteristics of hyaluronic acid hydrogels on in vitro neocartilage formation by mesenchymal stem cells. Biomaterials. 2009;30(26):4287–96. https://doi.org/10.1016/j.biomaterials.2009.04.040.
35. Sridhar BV, Brock JL, Silver JS, Leight JL, Randolph MA, Anseth KS. Development of a cellularly degradable PEG hydrogel to promote articular cartilage extracellular matrix deposition. Adv Healthcare Mater. 2015;4(5):702–13. https://doi.org/10.1002/adhm.201400695.
36. Langer R, Conn H, Vacanti J, Haudenschild C, Folkman J. Control of tumor growth in animals by infusion of an angiogenesis inhibitor. Proc Natl Acad Sci U S A. 1980;77(7):4331–5.
37. Moses MA, Sudhalter J, Langer R. Identification of an inhibitor of neovascularization from cartilage. Science. 1990;248(4961):1408–10.
38. Deveza L, Choi J, Lee J, Huang N, Cooke J, Yang F. Polymer-DNA nanoparticle-induced CXCR4 overexpression improves stem cell engraftment and tissue regeneration in a mouse hindlimb ischemia model. Theranostics. 2016;6(8):1176–89. https://doi.org/10.7150/thno.12866.
39. Watt SM, Gullo F, van der Garde M, Markeson D, Camicia R, Khoo CP, et al. The angiogenic properties of mesenchymal stem/stromal cells and their therapeutic potential. Br Med Bull. 2013;108(1):25–53. https://doi.org/10.1093/bmb/ldt031.
40. Tao H, Han Z, Han ZC, Li Z. Proangiogenic features of mesenchymal stem cells and their therapeutic applications. Stem Cells Int. 2016;2016:1314709. https://doi.org/10.1155/2016/1314709.
41. Goodpaster T, Legesse-Miller A, Hameed MR, Aisner SC, Randolph-Habecker J, Coller HA. An immunohistochemical method for identifying fibroblasts in formalin-fixed, paraffin-embedded tissue. J Histochem Cytochem. 2008;56(4):347–58. https://doi.org/10.1369/jhc.7A7287.2007.
42. Zara JN, Siu RK, Zhang X, Shen J, Ngo R, Lee M, et al. High doses of bone morphogenetic protein 2 induce structurally abnormal bone and inflammation in vivo. Tissue Eng A. 2011;17(9-10):1389–99. https://doi.org/10.1089/ten.tea.2010.0555.
43. Harada N, Watanabe Y, Sato K, Abe S, Yamanaka K, Sakai Y, et al. Bone regeneration in a massive rat femur defect through endochondral ossification achieved with chondrogenically differentiated MSCs in a degradable scaffold. Biomaterials. 2014;35(27):7800–10. https://doi.org/10.1016/j.biomaterials.2014.05.052.
44. Bikram M, Fouletier-Dilling C, Hipp JA, Gannon F, Davis AR, Olmsted-Davis EA, et al. Endochondral bone formation from hydrogel carriers loaded with BMP2-transduced cells. Ann Biomed Eng. 2007;35(5):796–807. https://doi.org/10.1007/s10439-007-9263-4.